Coupling between octahedral rotations and local polar displacements in WO_3/ReO_3 superlattices

Joseph T. Schick
Department of Physics, Villanova University, Villanova, Pennsylvania 19085, USA

Lai Jiang, Diomedes Saldana-Greco, and Andrew M. Rappe
The Makineni Theoretical Laboratories, Department of Chemistry, University of Pennsylvania, Philadelphia, Pennsylvania 19104-6323, USA
(Received 14 January 2014; published 13 May 2014)

We model short-period superlattices of WO_3 and ReO_3 with first-principles calculations. In fully relaxed superlattices we observe that octahedral tilts about an axis in the planes of the superlattices do not propagate from one material, despite the presence of the corner-shared oxygen atoms. However, we find that octahedral rotation is enhanced within WO_3 layers in cases in which strain couples with native antiferroelectric displacements of tungsten within their octahedral cages. Resulting structures remain antiferroelectric with low net global polarization. Thermodynamic analysis reveals that superlattices with sufficiently thick ReO_3 layers, the absolute number being three or more layers and the Re fraction $\geqslant 50\%$, tend to be more stable than the separated material phases and also show enhanced octahedral rotations in the WO_3 layers.

DOI: 10.1103/PhysRevB.89.195304 PACS number(s): 68.65.Cd, 73.21.Cd, 77.84.Bw, 77.80.bn

I. INTRODUCTION

Perovskites and related materials offer a wide variety of electronic, magnetic, and structural properties, along with couplings between these properties that can form the basis for numerous technological applications. In most cases, the structures of real perovskites deviate from the ideal case, most commonly in the form of coherent rotations of the octahedra in the crystal [1]. These rotations break cubic symmetry and typically require changes in the primitive lattice vectors, as well. Further symmetry reductions result from other changes in the structure, including Jahn-Teller and breathing mode distortions of the octahedra, and displacements of the *A* or *B* site cations.

Concomitant with the structural deviations are changes in the electronic, magnetic, and optical properties of the materials. The size of the semiconducting gap can be correlated with the degree of octahedral tilt in families of perovskites. For example, the metal-insulator transition temperature is correlated with the degree of octahedral tilt in rare-earth nickelates [2]. There is a growing literature on the relationships between octahedral tilting and properties of interest including Jahn-Teller distortions and cation ordering [3], ferroelectricity [4], and multiferroicity in perovskite layered phases and superlattices. The emergence of spontaneous polarization in short period perovskite superlattices due to the combination of two nonpolar rotation patterns, hybrid improper ferroelectricity, has been recently discussed as a route to creating multifunctional materials [5,6].

Because these useful material properties couple to octahedral tilting, there has been an effort to study the ways in which tilting can be adjusted, by creating interfaces or layered structures or by applying strain or electric or magnetic fields. Octahedral tilting is the primary way perovskites respond to applied strains because the octahedra are relatively rigid, due to the covalent *B*-O bonding [7,8]. However, the exact structure of any perovskite is a result of the interplay between the ionic and covalent nature of the bonding between the *A* and *B* cations and the O anions.

In a layered heterostructure, the tilts and rotations vary with distance from the interface, converging to bulk values. In addition, tilts and rotations will be affected by strains. The effect of epitaxial strain, in particular, has been previously investigated in theoretical studies [9,10], including determination of phase diagrams for numerous perovskites [10]. Strain-induced changes in bond lengths and angles were investigated experimentally in $LaNiO_3$ on $SrTiO_3$ and $LaAlO_3$, with a first-principles analysis demonstrating the ability to access structural phase changes in the response to tensile strain [11].

The dependence of tilt and rotation with respect to distance from a perturbation in $La_{0.75}Ca_{0.25}MnO_3$ and $SrRuO_3$ was recently investigated by distorting a single layer of the bulk material, while relaxing the remaining atoms but fixing the in-plane lattice parameters to mimic the effect of a substrate [12]. These calculations show that $La_{0.75}Ca_{0.25}MnO_3$ sustains out-of-plane tilts for a few layers, and that if the material is biaxially compressively strained, the imposed tilt results in a larger deep-layer tilt and a smaller in-plane rotation than found in the same biaxially, compressively strained material without an imposed tilt layer [12]. However, in $SrRuO_3$ the authors show that imposed tilts have no long-range propagation into the material, whether or not it is biaxially strained [12]. In both cases, the distance to attain the deep-layer behavior is very short, of the order of one or two layers.

Certain binary transition-metal oxides form in a perovskite-like structure, forming BO_6 octhedra with empty *A* sites. ReO_3 and WO_3 possess this structure and allow us to focus on the BO_6 octahedra exclusively. WO_3 is a monoclinic insulator at room temperature. WO_3 undergoes numerous structural phase transitions both above and below room temperature, with the triclinic phase stable below 290 K, for example [13]. The tungsten atoms in WO_3 are displaced from their octahedral centers, in an antiferroelectric pattern [14]. ReO_3 is a conductor with cubic symmetry at room temperature and below [15]. Numerous *ab initio* studies of ReO_3 and WO_3 have been carried out [16–20], and the link between the WO_3 band gap and the polar distortion of the W atoms has been investigated [16,17]; the reduction in energy of the occupied states is cited as the driver of the polar displacements. In a recent theoretical investigation of the surfaces of WO_3, ReO_3,

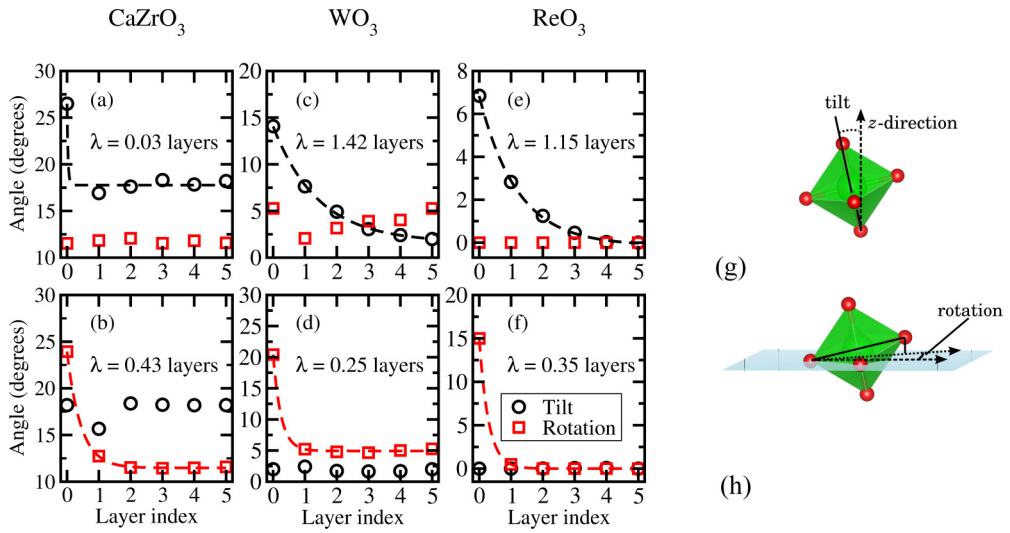

FIG. 1. (Color online) Octahedral tilt and rotation angles in each plane along the long axis of $2 \times 2 \times 6$ supercells of $CaZrO_3$, WO_3, and ReO_3. The layer zero equatorial oxygen atoms were held fixed to maintain an excess octahedral tilt [(a), (c), and (e)] or octahedral rotation [(b), (d), and (f)] alone. The equatorial oxygen atoms in layer five were held fixed to maintain calculated bulk tilt and rotation angles. All other O atoms and all A and B cation locations were relaxed. The characteristic decay lengths λ are computed by fitting to Eq. (1) and given in units of the layer index. (g) Tilt angles are the angles between the supercell c axis and the polar axis of the octahedra. (h) Rotation angles evaluated by averaging the angles between the supercell a and b axes and ab-projected line of the nearest octahedral O-O axis. The differences between the lattice directions and the Cartesian axes in this work are small and are ignored.

and surface layers of WO_3 on ReO_3 and ReO_3 on WO_3, it was found that layering is the preferred ordering for Re and W in bulk $WReO_6$ [21].

In this paper we demonstrate that WO_3 and ReO_3 both possess longer characteristic decay lengths for out-of-plane tilts than the reference material $CaZrO_3$, but their in-plane rotation characteristic decay lengths are comparable. We also present results for superlattices and compare their tilt and rotation behaviors to the pure materials. We determine that the antiferroelectric displacements of tungsten and the superlattice strain combine to influence the tilt and rotation angles.

II. COMPUTATIONAL DETAILS

Density functional theory (DFT) calculations were performed with the Perdew-Burke-Ernzerhof (PBE) parametrization of the generalized gradient approximation (GGA). Norm-conserving nonlocal pseudopotentials were generated with the OPIUM code [22]. Calculations were performed with QUANTUM ESPRESSO [23]. The energy cutoff for plane waves was 680 eV. A $2 \times 2 \times 2$ Monkhorst-Pack k-point mesh [24] was used for relaxing bulk materials; a $6 \times 6 \times 6$ grid was tested to ensure convergence. In four-layer supercells a $2 \times 2 \times 2$ k-point grid was used. In six- and eight-layer supercells a $2 \times 2 \times 1$ k-point sampling was employed. Ionic forces were converged to 0.0004 Ry/a_0 and pressures in full-cell relaxations were below 0.2 kbar. Electronic energy was converged to 10^{-8} Ry. Full structural convergence was tested in the four-layer superlattices with a $4 \times 4 \times 4$ k-point grid. The bulk ReO_3 valence band is composed of strongly delocalized Re d and O p states. It has been previously found in $LaNiO_3$, which is also metallic, that similarly delocalized states strongly screen the electron-electron interactions. From this screening it was concluded that Hubbard U and hybrid functionals cannot accurately represent the screening effects of these delocalized electrons [25]. For this reason we do not include these methods in this calculation.

III. RESULTS AND DISCUSSION

Imposing tilt on a single layer in $CaZrO_3$ [Fig. 1(a)] has little effect on the material. In a $CaZrO_3$ $2 \times 2 \times 6$ unit supercell, we held one layer fixed at the bulk tilt and rotation values, and tilted or rotated the oxygen cages on the opposite end. The rest of the atoms in the supercell were relaxed. The length of decay is characterized with an exponential fit. In Fig. 1(a) we imposed only a tilt on layer zero and fit the resulting tilt distribution with the expression

$$\theta(x) = \theta_\infty + (\theta_0 - \theta_\infty)e^{-x/\lambda}, \quad (1)$$

where θ is the tilt angle, x is the layer index, θ_∞ is the bulk tilt angle, θ_0 is the imposed tilt at the first layer, and λ is a characteristic length, in units of layers, for the decay of the tilts and rotations into the bulk. In Fig. 1(b) the same analysis is displayed for the imposed rotation angle. Surprisingly, we find that although tilts involve displacement of the apical oxygen atoms, which are shared by neighboring layers, the characteristic length λ_{tilt} in $CaZrO_3$ is very short. Perhaps equally surprising is the fact that $\lambda_{\text{rotate}} > \lambda_{\text{tilt}}$ in $CaZrO_3$; rotations decay more gradually than tilts, though both are quite rapidly decaying.

There is apparently only a limited relationship between the tilt or rotation in one layer and the next. However, we observe in Figs. 1(c) through 1(f) that the characteristic decay lengths for tilt (but not rotation) angles in WO_3 and ReO_3 are significantly longer than for $CaZrO_3$ and that $\lambda_{\text{rotate}} < \lambda_{\text{tilt}}$ in the BO_3 materials.

TABLE I. The calculated parameters of fully relaxed $2 \times 2 \times 2$ unit cells of ReO_3 and WO_3. (Experimental values are in parentheses.) Tilt and rotation are defined in Fig. 1.

Parameter	ReO_3	WO_3
a	7.55 (7.50)[a] Å	7.46 (7.31)[b] Å
b	–	7.56 (7.53)[b] Å
c	–	7.75 (7.69)[b] Å
α	90° (90°)[a]	90° (88.9°)[b]
β	90° (90°)[a]	90.02° (90.9°)[b]
γ	90° (90°)[a]	90° (90.9°)[b]
Mean oct. tilt	0°	2°
Mean oct. rotation	0°	5°

[a]From Ref. [26].
[b]From Ref. [27].

Having established that tilt and rotation disturbances result in layer-to-layer correlations in these binary materials, we investigate superlattices that are more readily synthesized. Our superlattices are constructed from $2 \times 2 \times N$ pseudocubic unit cells. Each of the N layers is composed of either four WO_6 or four ReO_6 octahedra. The lattice and all the atomic coordinates are fully relaxed in these calculations. Calculated lattice parameters of the bulk materials are listed in Table I.

The rotation and tilt profiles of the six-layer superlattices are displayed in Fig. 2. For systems with half or more ReO_3 [Figs. 2(a)–2(c)], the ReO_3 exerts compressive strain on the WO_3 (discussed below), leading to enhanced rotation angles ≈8° in the WO_3 layers. For the two cases with more W than Re, the rotations are near the bulk value ≈5°. In all cases, rotations are zero in the ReO_3 layers, with an abrupt change in the octahedral rotation angle across the boundary. The single-layer change in the rotation angle across the superlattice boundaries is consistent with the short characteristic length for the decay of rotations (small values of λ_{rotate}) observed previously.

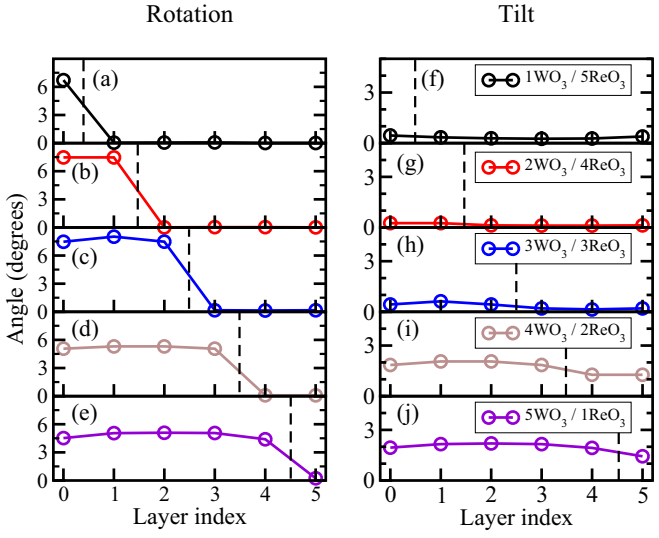

FIG. 2. (Color online) The rotation [(a)–(e)] and tilt [(f)–(j)] angles of six-layer WO_3/ReO_3 fully relaxed superlattices are presented as a function of layer index. The vertical dashed line indicates the boundary between WO_3 (to the left) and ReO_3 (to the right). ReO_3 layers all have nearly zero rotation. The superlattices with three or fewer WO_3 layers have rotation angles ≈8°. The rotation in majority WO_3 superlattices are near the bulk values ≈5°. All WO_3 tilt angles are small, nearly zero in majority ReO_3 superlattices.

Octahedral tilt angles [Figs. 2(f)–2(j)] are anticorrelated with rotation angles in WO_3; the systems with larger rotations have lower tilts. However, unlike the results for rotations, the ReO_3 layers also exhibit nonzero tilts for the majority WO_3 superlattices. The penetration of tilt angles through these superlattices is consistent with the longer characteristic length for tilts within both materials (larger values of λ_{tilt}).

The increase of rotation angles in superlattices with more ReO_3 arise largely from superlattice strain, with some contribution due to WO_3 polar displacements. As seen in Table I, two of the WO_3 lattice parameters differ from ReO_3 by 1% or 2% with the b lattice parameter nearly identical. The in-plane lattice parameters of the superlattices discussed here remain close to that of bulk ReO_3. Because ReO_3 has a much larger bulk modulus (≈200 GPa) [28,29] than WO_3 (≈41 GPa) [30], the domination of the superlattice in-plane lattice parameters by ReO_3 is not surprising. The long dimension in bulk WO_3 is a result of minimal tilt ≈2° and the slight elongation of the octahedral axis closest to the direction of the polar (antiferroelectric) displacement of the W ions.

The superlattices were initially set up with the ab planes of bulk WO_3 forming surfaces of contact. The lattice parameters (Table I) lead us to expect a tensile strain on the WO_3 layers, which would reduce the rotation angle, the opposite of the observed results. In bulk WO_3, calculated W displacements from the geometric centers of their octahedral cages are generally toward octahedral edges and make angles ≈31° with respect to the c axis. However, in the cases with increased rotation (those with more ReO_3), the directions of the antiferroelectric polar displacements of the W cations make angles from ≈60° to 90° with respect to the c axis, increasing with the fraction of ReO_3. (See Table II.) This results in the long axis of the WO_3 octahedra also lying in the superlattice planes, requiring the WO_3 octahedra to rotate more strongly to fit within the lattice.

The average magnitude of local polar (antiferrelectric) displacement in the ReO_3 layers increases as the Re fraction decreases and as the superlattice thickness decreases. Superlattices with a single ReO_3 layer have the largest Re displacements. The directions of Re displacements are close to the long axis of the superlattice. The average magnitude of local polar displacements of W atoms are ≈0.2 Å, decreasing to ≈0.15 Å for the highest Re fractions. The W polar displacement angle to the superlattice axis varies with Re polar displacement at the interface plane (Fig. 3), lying completely in the plane for the highest Re fraction (Table II). The polar displacement angles throughout the WO_3 layers differ by $<1°$ from the surface value.

To test the effect of the initial conditions on the fully relaxed final structures and formation energies of the superlattices, we also created four- and six-layer superlattices with the bc planes of bulk WO_3 forming the initial contact surfaces. All possible m/n superlattices were formed. After full relaxation, the energies of the test superlattices were higher than the ab-oriented superlattices, ≈0.03 eV for the four-layer and ≈0.07 eV for six-layer superlattices. The lattice parameters are controlled by

TABLE II. Average antiferroelectric displacements of Re in ReO_3 surface layers $\overline{P}_{Re}$ decrease with increasing ReO_3 fraction. The average angle between the W displacements and the axis of the superlattice in WO_3 surface layers $\overline{\theta}_{P_z,W}$ generally increases with increasing ReO_3 fraction for a given superlattice thickness.

No. of superlattice layers	No. of ReO_3 layers	$\overline{P}_{Re}$ (Å)	$\overline{\theta}_{P_z,W}$ (deg)
2	1	0.118	41
4	1	0.128	40
4	2	0.071	60
4	3	0.022	90
6	1	0.137	37
6	2	0.104	44
6	3	0.034	75
6	4	0.039	73
6	5	0.019	90
8	1	0.140	35
8	2	0.102	44
8	3	0.054	62
8	4	0.061	60
8	5	0.034	74
8	6	0.019	88
8	7	0.020	89

the ReO_3 material, as discussed above. In these tests, rotations do not penetrate into the ReO_3 layers and the tilt and rotation profiles are consistent with the superlattices explored above. In these test configurations, when there are odd numbers of WO_3 layers, the initial condition has a net polar shift of W cations along the *b* direction, transverse to the axis of the superlattice. (The initial polar displacement vectors' largest components remain along the *c* direction.) These net displacements vanish in the fully relaxed $(WO_3)_5/(ReO_3)_1$ and $(WO_3)_3/(ReO_3)_1$ superlattices but persist in the Re-dominated superlattices. The W-rich superlattices also have polar displacements closer to the superlattice direction, consistent with the lower energy superlattices.

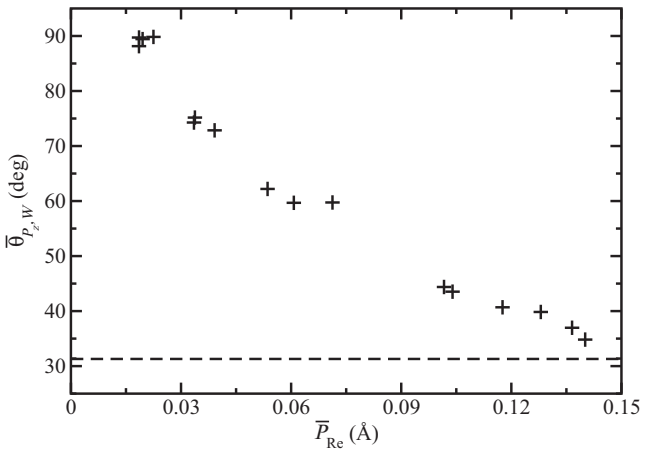

FIG. 3. The average angle to the *c* axis of polar displacements in WO_3 interface planes vary with the average magnitude of antferroelectric polar displacements induced in the ReO_3 interface planes. The horizontal dashed line indicates the average polar displacement angle in bulk WO_3 (≈31°). See Table II for detailed comparison of the data.

Above we observed that tilts penetrate across the interfaces (Fig. 2), consistent with the larger λ_{tilt} in these materials. As a result, when ReO_3 makes up the majority of the superlattice, tilts are suppressed within the WO_3 layers. Furthermore, when ReO_3 is the majority material, the induced polar displacements in ReO_3 layers are smallest and the polar displacements in WO_3 lie in superlattice layers. We tested the response of the polar displacements in bulk WO_3 to biaxial strain, of the same amount as in the $(WO_3)_1/(ReO_3)_7$ superlattice, and found that the angle of the polarization increases only to ≈40° (in comparison to the bulk ≈31° and the superlattice ≈89°). Strain alone is not enough to cause the large in-plane polar displacement in WO_3.

Table II shows that the largest antiferroelectric Re displacements at the surface occur when there are one or two ReO_3 layers. The superlattices with three or more ReO_3 layers have very small surface Re displacements and also have W displacements lying closer to the superlattice planes, as noted above. Furthermore, the W displacement angles in all layers in any given superlattice remain close to the same value found at the surface. Evidently, the energy cost for displacing the Re cations is large in comparison to the energy cost to reorient the W displacements into the superlattice planes. To estimate this energy, the computed energy required for a 0.14 Å antiferroelectric displacement in bulk ReO_3, corresponding to the maximum displacement found in the present calculations, is ≈0.08 eV per four formula units. As will be observed below, this is small in comparison to interface and strain energies.

Hybrid improper ferroelectrics have recently been highlighted as a possible means to create new multifunctional materials [5,6]. The mechanism induces a spontaneous polarization through coupling to two nonpolar rotational modes enabled by creation of $AA'BO_3$ double-perovskites [31] or Ruddleston-Popper phases. The induced polarization in hybrid improper ferroelectrics is perpendicular to the layering. We note that the local polarization of the WO_6 octahedra lies in or close to the layers of Re-majority superlattices (Table II), which we have concluded is a result of strain and a microscopic interaction at interfaces, a mechanism perhaps related to that discussed for hybrid improper ferroelectrics.

Because there is coupling between the superlattice layers and the orientation of the W polar displacements, we computed total polar displacements by summing all the displacement vectors for each type of *B* cation in each superlattice. Total displacements are all of the order 10^{-3} Å and less in the low energy superlattices. These displacements are negligible relative to the typical polar displacements of the W and Re atoms. The lack of overall polarization in our calculations is perhaps related to the fact that all the superlattices are conductors. In Fig. 4 the densities of states (DOS) demonstrate the superlattices are metallic, with an apparently strong contribution from ReO_3-like states at the Fermi level. The DOS projected onto metal-*d* and O-*p* states for the $(WO_3)_3/(ReO_3)_3$ superlattice (Fig. 5) shows that hybridized Re-*d* and O-*p* states are the strongest contributions to the DOS at the Fermi energy. Figure 5 shows the strong hybridization between O *p* states and Re *d* states. Such hybridization has previously been shown to result in screening of the electron-electron interaction that

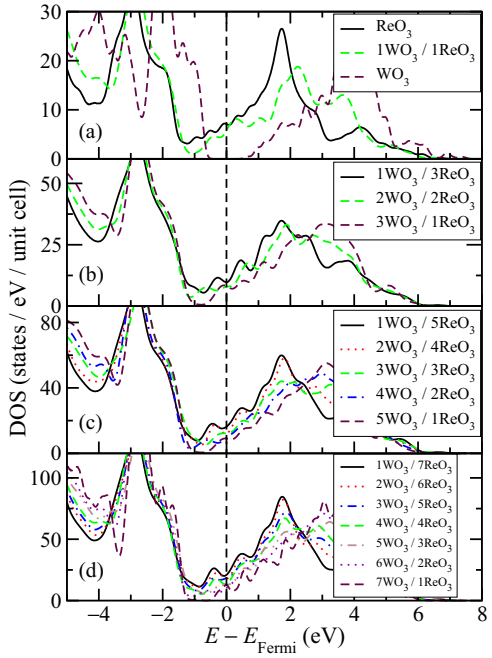

FIG. 4. (Color online) The densities of states for (a) two-layer, (b) four-layer, (c) six-layer, and (d) eight-layer superlattices are compared with the density of states of (a) bulk BO_3 materials. In all calculations there were four formula units in each layer. We observe that all the superlattices possess Fermi levels within bands. In the cases with lowest Re fraction, there appears to be a gap opening below the Fermi energy.

cannot be properly captured with Hubbard U nor with hybrid density functionals [25], justifying our avoidance of applying such methods in this calculation.

Projecting the densities of states into individual layers of the superlattice (Fig. 6) shows that the states at the Fermi

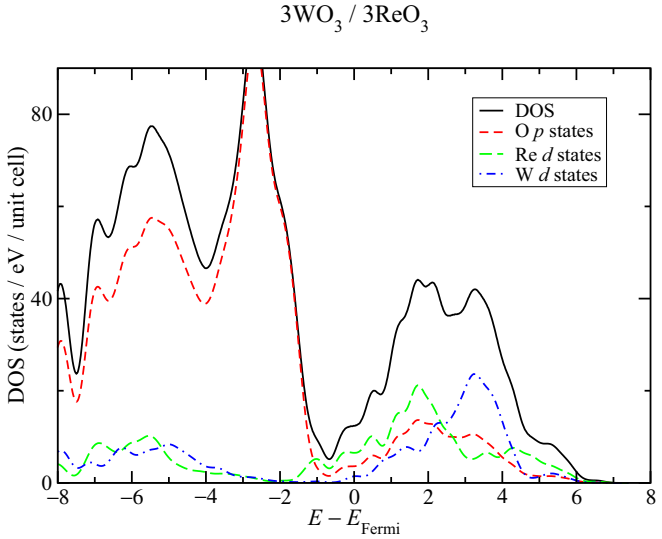

FIG. 5. (Color online) The densities of states projected onto O-p and metal-d states in the $(WO_3)_3/(ReO_3)_3$ superlattice shows that the states just around the Fermi energy are made up of hybridized Re-d and O-p states.

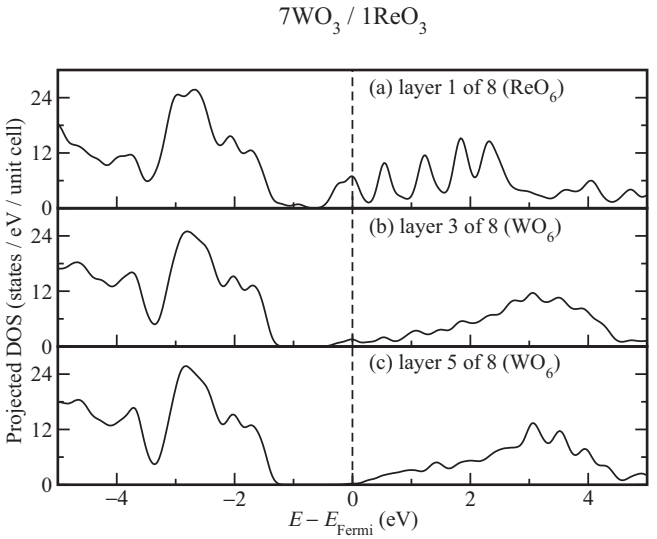

FIG. 6. Projected densities of states for the $(WO_3)_7/(ReO_3)_1$ superlattice are displayed for three layers within the superlattice. (a) Projection on the ReO_6 octahedra, (b) projection on the WO_6 octahedra of the second layer after rhenium layer, and (c) projection on the WO_6 octahedra on the layer farthest from the rhenium layers.

energy are due primarily to the ReO_3 layer of the superlattice, with the density of states at the Fermi level decreasing rapidly with distance from the rhenium layer. We expect reduced conductivity in superlattices with respect to bulk ReO_3 because the total density of states at the Fermi energy is lower than in bulk ReO_3.

The formation energies of the $(WO_3)_m/(ReO_3)_n$ superlattices with respect to equivalent amounts of the bulk materials,

$$E_f(m,n) = E_{\text{total}} - mE_{WO_3} - nE_{ReO_3}, \qquad (2)$$

shows that some superlattices are more stable than the separated bulk phases. Here E_{WO_3} and E_{ReO_3} are the formation energies for single layers of the corresponding bulk materials. The data points in Fig. 7 display $E_f(m,n)$ for each superlattice. We observe that higher rhenium fractions are generally more favorable than lower, with a preference for three rhenium layers as a minimum. The possible sources of these energy deviations are the energy associated with strains of the materials in the superlattices and the energy to create the interfaces. We parametrize the superlattice formation energy in terms of the energy costs to strain bulk layers of both WO_3 and ReO_3 ($\Delta E^{\text{str}}_{WO_3}$ and $\Delta E^{\text{str}}_{ReO_3}$) and to create the interfaces ΔE_{int} with the model

$$E_f(m,n) = \Delta E_{\text{int}} + m\Delta E^{\text{str}}_{WO_3} + n\Delta E^{\text{str}}_{ReO_3}, \qquad (3)$$

where m and n are the numbers of layers of WO_3 and ReO_3, respectively. The results fitting this model are displayed as straight lines in Fig. 7. The fitting parameters in Table III show that reducing the number of layers of WO_3 and increasing the number of layers of ReO_3 are both more energetically favorable. The majority of the energy change is due to distortion of the ReO_3 layers, as indicated by the magnitude of $\Delta E^{\text{str}}_{ReO_3}$ in comparison to $\Delta E^{\text{str}}_{WO_3}$. The energy reduction in

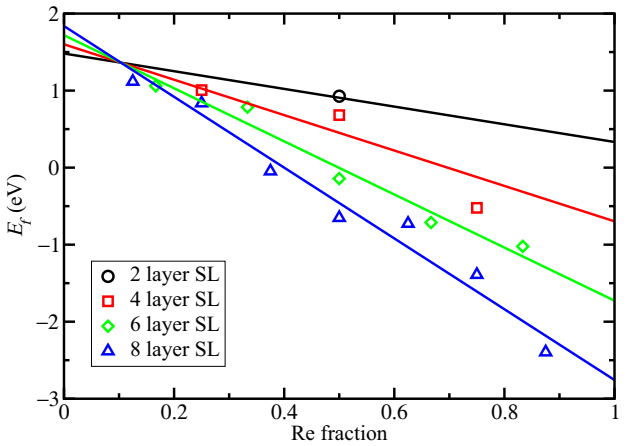

FIG. 7. (Color online) The formation energies E_f relative to separated WO_3 and ReO_3 phases [calculated from Eq. (2)] for all superlattice calculations are plotted as a function of Re concentration. Generally superlattices consisting of larger numbers of layers of ReO_3 are more stable than those with fewer layers. The straight lines are energies calculated from the model [Eq. (3)] using the values in Table III.

increasing the Re fraction by changing a layer of WO_3 to ReO_3 (0.574 eV) is also large in comparison to the interface energy providing a reason for ReO_3 to form thick layers, which is consistent with the previous calculation finding that layering is the preferred order in $WReO_6$ [21].

As noted in the discussion for Table II, increasing ReO_3 fraction also decreases the local polarization of ReO_3 and increases the angle to the superlattice long axis of the local polarization of WO_3. We also tried including polar displacement in the energy model but found that the fit quality was reduced, suggesting that the strain effects are dominant and that changes in polarization are a response to the constraints imposed by the superlattice. The energy reduction from increasing ReO_3 fraction is apparently assisted by the ability of the tungsten layers to more readily accommodate strain through octahedral rotations, which also relates to the lower bulk modulus of WO_3. For the superlattices in which ReO_3 is the majority material, the energies are lower than the bulk phases, suggesting that these superlattices may be experimentally feasible, either through film deposition or bulk material segregation.

TABLE III. The parameters obtained by fitting Eq. (3) with the energies obtained from DFT results.

Parameter	Value (per four formula units)
ΔE_{int}	1.363 eV
$\Delta E^{\text{str}}_{WO_3}$	0.059 eV/layer
$\Delta E^{\text{str}}_{ReO_3}$	−0.515 eV/layer

IV. CONCLUSION

In summary, we have found that there is a stronger layer-to-layer correlation between tilt angles in the binary transition-metal oxides WO_3 and ReO_3 than is found in most studies of ternary transition-metal oxides. Rotation angles are enhanced in some superlattices because antiferroelectric polar distortions of the WO_6 octahedra cause them to couple with the layering of the material, reminiscent of the hybrid improper ferroelectricity concept [32]. However, net global polarization is low. We find that short-period superlattices are stable relative to bulk XO_3 compounds when the ReO_3 layer thickness is large enough and when ReO_3 is the majority species. This stability suggests that creation of these short-period superlattices will be experimentally realizable.

ACKNOWLEDGMENTS

The authors gratefully acknowledge their support. J.T.S. was supported by a sabbatical granted by Villanova University. L.J. was supported by the Air Force Office of Scientific Research under Grant No. FA9550-10-1-0248. D.S.G. was supported by the Department of Energy Office of Basic Energy Sciences, under Grant DE-FG02-07ER15920. A.M.R. was supported by the Office of Naval Research, under Grant N00014-12-1-1033. Computational support was provided by the High Performance Computing Modernization Office of the Department of Defense, and the National Energy Research Scientific Computing Center of the Department of Energy.

[1] A. M. Glazer, Acta Crystallogr. Sect. B **28**, 3384 (1972).
[2] M. L. Medarde, J. Phys.: Condens. Matter **9**, 1679 (1997).
[3] M. Lufaso and P. Woodward, Acta Crystallogr. Sect. B **60**, 10 (2004).
[4] N. A. Benedek and C. J. Fennie, J. Phys. Chem. C **117**, 13339 (2013).
[5] N. A. Benedek and C. J. Fennie, Phys. Rev. Lett. **106**, 107204 (2011).
[6] N. A. Benedek, A. T. Mulder, and C. J. Fennie, J. Solid State Chem. **195**, 11 (2012), Polar Inorganic Materials: Design Strategies and Functional Properties.
[7] J. B. Goodenough, Phys. Rev. **100**, 564 (1955).
[8] P. Garcia-Fernandez, J. Aramburu, M. Barriuso, and M. Moreno, J. Phys. Chem. Lett. **1**, 647 (2010).
[9] A. T. Zayak, X. Huang, J. B. Neaton, and K. M. Rabe, Phys. Rev. B **74**, 094104 (2006).
[10] O. Diéguez, K. M. Rabe, and D. Vanderbilt, Phys. Rev. B **72**, 144101 (2005).
[11] S. J. May, J.-W. Kim, J. M. Rondinelli, E. Karapetrova, N. A. Spaldin, A. Bhattacharya, and P. J. Ryan, Phys. Rev. B **82**, 014110 (2010).
[12] J. He, A. Borisevich, S. V. Kalinin, S. J. Pennycook, and S. T. Pantelides, Phys. Rev. Lett. **105**, 227203 (2010).
[13] E. Salje, Acta Crystallogr. Sect. B **33**, 574 (1977).
[14] K. M. Rabe, in *Functional Metal Oxides* (Wiley-VCH, Berlin, 2013), pp. 221–244.
[15] W. Biltz, G. A. Lehrer, and K. Meisel, Z. Anorg. Allg. Chem. **207**, 113 (1932).

[16] F. Corà, M. G. Stachiotti, C. R. A. Catlow, and C. O. Rodriguez, J. Phys. Chem. B **101**, 3945 (1997).
[17] G. A. de Wijs, P. K. de Boer, R. A. de Groot, and G. Kresse, Phys. Rev. B **59**, 2684 (1999).
[18] A. D. Walkingshaw, N. A. Spaldin, and E. Artacho, Phys. Rev. B **70**, 165110 (2004).
[19] F. Wang, C. Di Valentin, and G. Pacchioni, J. Phys. Chem. C **115**, 8345 (2011).
[20] Y. Ping, D. Rocca, and G. Galli, Phys. Rev. B **87**, 165203 (2013).
[21] S. Ling, D. Mei, and M. Gutowski, Catal. Today **165**, 41 (2011).
[22] OPIUM pseudopotential generating package, http://opium.sourceforge.net/.
[23] P. Giannozzi *et al.*, J. Phys.: Condens. Matter **21**, 395502 (2009).
[24] H. J. Monkhorst and J. D. Pack, Phys. Rev. B **13**, 5188 (1976).
[25] G. Gou, I. Grinberg, A. M. Rappe, and J. M. Rondinelli, Phys. Rev. B **84**, 144101 (2011).
[26] J.-E. Jørgensen, J. D. Jorgensen, B. Batlogg, J. P. Remeika, and J. D. Axe, Phys. Rev. B **33**, 4793 (1986).
[27] P. Woodward, A. Sleight, and T. Vogt, J. Phys. Chem. Solids **56**, 1305 (1995).
[28] T. P. Pearsall and L. A. Coldren, Solid State Commun. **18**, 1093 (1976).
[29] R. E. Benner, E. M. Brody, and H. R. Shanks, J. Solid State Chem. **22**, 361 (1977).
[30] W. A. Crichton, P. Bouvier, and A. Grzechnik, Mater. Res. Bull. **38**, 289 (2003).
[31] J. M. Rondinelli and C. J. Fennie, Adv. Mater. **24**, 1918 (2012).
[32] V. Dvořák, Ferroelectrics **7**, 1 (1974).